Chapter 2

Nonlinear Time Series Analysis and Higher Order Spectra

In this chapter, examples are presented to show how phase couplings of frequency components can be used to detect quadratic and cubic nonlinearities. First, Fourier analysis and higher order spectral moments are introduced. Several spectral moments are defined and applied to the identification of linear and nonlinear time series. Two nonlinear systems are then solved numerically and by perturbation techniques. The coupled frequencies in the numerical solution are identified by higher order spectra and related to the frequencies present in the perturbation solution. A new method for visualizing the tricoherence is presented and its benefits are cited. Finally, time/frequency analysis is introduced by defining the continuous wavelet transform. A computer algorithm for computing the wavelet transform is verified and certain advantages of wavelet analysis over Fourier analysis in the characterization of nonlinear nonstationary time series are discussed. The higher order spectral moments are then defined in terms of wavelet coefficients. The ability of the wavelet-based spectral moments to characterize intermittent nonlinear couplings is demonstrated using a numerical example.

2.1 Frequency and Phase Couplings in Quadratic and Cubic Systems

Single Frequency Excitation of a Quadratic System

As an example of a quadratic system, we consider the input-output relation

$$y(t) = x(t) + x^2(t) \tag{2.1}$$

For a single frequency excitation $x(t)$ of the form

$$x(t) = Cos(2\pi f_0 t + \phi_0) \tag{2.2}$$

the resulting output, $y(t)$, consists of a DC component and two quadratically phase coupled components and is written as

$$y(t) = \frac{1}{2} + Cos(2\pi f_0 t + \phi_0) + \frac{1}{2}Cos(2\pi 2 f_0 t + 2\phi_0) \tag{2.3}$$

The first harmonic component is identical to the input function in both phase and frequency; the second harmonic component has twice the frequency and its phase is equal to twice that of the input. The two harmonic components are referred to as "phase coupled" because the phase and frequency of the output are related to the the phase and frequency of the input [17].

Multifrequency Excitation of a Quadratic System

When subjected to a multifrequency input of the form

$$x(t) = Cos(2\pi f_0 t + \phi_0) + Cos(2\pi f_1 t + \phi_1) \tag{2.4}$$

the quadratic system presented in Eq. 2.1 yields

$$
\begin{aligned}
y(t) = 1 &+ Cos(2\pi f_0 t + \phi_0) + Cos(2\pi f_1 t + \phi_1) + \\
&\frac{1}{2}Cos(2\pi 2 f_0 t + 2\phi_0) + \frac{1}{2}Cos(2\pi 2 f_1 t + 2\phi_1) + \\
&Cos(2\pi(f_0 + f_1)t + \phi_0 + \phi_1) + Cos(2\pi(f_0 - f_1)t + (\phi_0 - \phi_1))
\end{aligned} \tag{2.5}
$$

In this case, the output consists of one DC component and six phase coupled harmonic components. The frequency components in $y(t)$, f_0, f_1, $2f_0$, $2f_1$, $f_0 + f_1$, and $f_0 - f_1$ are coupled to the phases of the frequency components of the input. Particularly, in each component, both the frequency and the phase bear the same relationship to the original input e.g. when frequency doubling occurs, phase doubling also occurs and when frequency summation occurs, phase summation also occurs, etc. It should be clear that frequency/phase doubles, sums, and differences are telltale signs of a nonlinear system [17].

Single Frequency Excitation of a Cubic System

As an example of a cubic system, we consider the input-output relation

$$y(t) = x(t) + x^3(t) \tag{2.6}$$

When subjected to the single frequency harmonic excitation of the form,

$$x(t) = Cos(2\pi f_0 t + \phi_0) \tag{2.7}$$

the output

$$y(t) = \frac{1}{4}(7Cos(2\pi f_0 t + \phi_0) + Cos(2\pi 3 f_0 t + 3\phi_0)) \tag{2.8}$$

contains two frequency components, f_0 with phase ϕ_0, and $3f_0$ with phase $3\phi_0$. Again, the cubically generated frequency component shares the same relationship as the phase (tripling) to the original frequency.

2.2 Fourier-Based Analysis Tools

In this section, the Fourier transform is introduced. Higher order spectra (HOS) are defined in terms of Fourier coefficients. Spectral moments are used to identify nonlinearities in two different systems. Finally, a new method of plotting the tricoherence is presented.

2.2.1 Continuous and Discrete Fourier Transform

The continuous Fourier transform defined as

$$X(\omega) = \int_{-\infty}^{\infty} x(t)e^{-i\omega t}dt \tag{2.9}$$

is used to map one function, $x(t)$, onto the set of complex sinusoid basis functions, $e^{-i\omega t}$. An inverse Fourier transform can also be defined as

$$x(t) = \frac{1}{2\pi}\int_{-\infty}^{\infty} X(\omega)e^{i\omega t}d\omega \tag{2.10}$$

and is used to map functions from the frequency domain back to the time domain. Together, these two operations form a Fourier transform pair [17]. The discrete Fourier transform is given by [17]

$$X[k] = \sum_{j=1}^{N} x[j]e^{-2\pi i(j-1)(k-1)/N} \tag{2.11}$$

and its inverse transform is written as [17]

$$x[j] = \frac{1}{N}\sum_{k=1}^{N} X[k]e^{2\pi i(j-1)(k-1)/N} \tag{2.12}$$

In the above equations, the real discrete time series, $x[j]$, is parameterized by index j where $j = 1, ..., N$, the frequency domain signal $X[k]$, is parameterized by index k where $k = 1, ..., N$, and the total number of points in the signal is N.

Limits are imposed on the frequency content of a discrete signal due to the sampling frequency and the total signal duration. The highest resolvable frequency under ideal conditions, referred to

as the Nyquist frequency, f_N, is half of the sampling frequency, f_s [17], i.e.

$$f_N = \frac{f_s}{2} \tag{2.13}$$

The frequency resolution is determined by the total duration of the signal, T, and the sampling frequency as [17]

$$\Delta f = \frac{f_s}{T} \tag{2.14}$$

2.2.2 Moment Functions and Moment Spectra

The auto-correlation function, $m_{xx}(\tau)$, of a stationary random process, $x(t)$, is defined in [18] as

$$m_{xx}(\tau) = E[x(t)x(t+\tau)] \tag{2.15}$$

where $E[\cdot]$ denotes the expected value operator. The autocorrelation is referred to as a "second order moment function" of $x(t)$ since it calls upon $x(t)$ twice [18]. The expected value operator represents ensemble averaging.

The Wiener-Khintchine theorem [18] relates the power spectrum $P_{xx}(f)$ (Fourier domain), to the autocorrelation function as

$$m_{xx}(\tau) \leftrightarrow P_{xx}(f) \tag{2.16}$$

where $\leftrightarrow$ denotes the Fourier transform operation. The power spectrum is likewise referred to as a "second order moment spectrum" [18]. For a stationary times series, the power spectrum can be calculated from the Fourier transform as

$$P_{xx}(f) = \lim_{T\to\infty} \frac{1}{T} E[X_T(f)X_T^*(f)] \tag{2.17}$$

where $X_T(f)$ is the Fourier transform over an interval T and the * represents the complex conjugate operation. When applied to a record, the quantity $P_{xx}(f)$, is simply an estimate of the power spectrum. A hierarchy of spectral moments can also be defined in the same manner [18]. Since the

power spectrum is a common operation, spectral moments of order > 2 are referred to as "higher order spectra" or HOS. Several of these spectral moments are introduced in the following sections. A more detailed description of the definitions and origins can be found in [18], [44], [45], and [46] and some of their references.

2.2.3 Fourier-Based Spectral Moments

Power Spectrum

The power spectrum, defined above and repeated here

$$P_{xx}(f) = \lim_{T\to\infty} \frac{1}{T} E[X_T(f) X_T^*(f)] \tag{2.18}$$

is a real positive quantity that gives a measure of the harmonic power as a function of frequency. As described in Section 2.2.1, the highest frequency of the power spectrum is limited by the sampling frequency. To illustrate the use of the power spectrum, a digitally sampled $10Hz$ sinusoid is shown in the top portion of Figure 2.1. Its power spectrum is shown in the bottom portion of the same figure. A peak, indicating harmonic power, appears at $10Hz$, and no other peaks are present.

A second example is shown in Figure 2.2. Here, a $10Hz$ sinusoid, a $15Hz$ sinusoid, and some additive white Gaussian noise (AWGN) are combined. A portion of the signal is shown in the top plot, and its power spectrum is shown in the bottom plot. Since broadband noise was added, power is present at all frequencies. Significant peaks at $10Hz$ and $15Hz$ indicate energy content at these frequencies.

Linear Coherence

The linear coherence is a measure of the linear coupling between two signals. It is defined as [18]

$$\gamma_{yx}^2(f) = \lim_{T\to\infty} \frac{1}{T} \frac{|E[X_T^*(f) Y_T(f)]|^2}{E[X_T(f) X_T^*(f)] E[Y_T(f) Y_T^*(f)]} \tag{2.19}$$

Based on Schwarz's inequality, it is bound in the interval of $[0, 1]$. A zero value indicates the absence of coupling. A high value indicates a strong coupling level. The linear coherence of an input-output

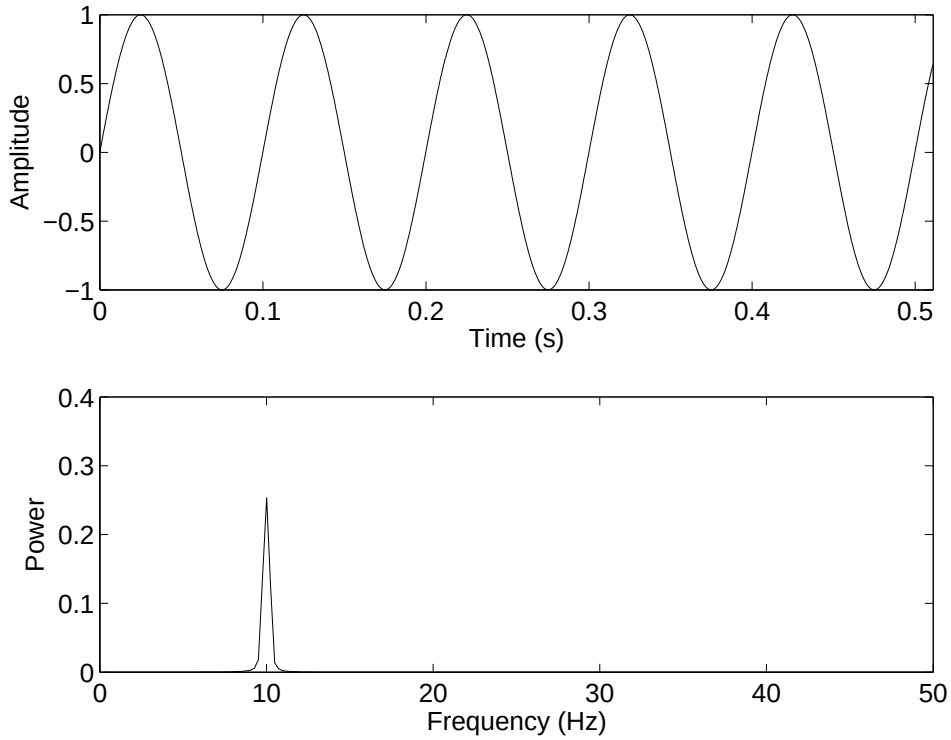

Figure 2.1: A portion of a $10Hz$ sinusoid is shown in the top of the figure. The power spectrum of the time series is shown in the bottom of the figure. Note the strong peak at $10Hz$.

system where a 10Hz signal is present in the input and phase coupled 10Hz and 20Hz frequency components in addition to white noise are present in the output is shown in Figure 2.3. The plot shows the expected high linear coupling level at the 10Hz component.

Auto-Bispectrum

The next higher order spectral moment to the power spectrum is the auto-bispectrum which is defined as [18]

$$B_{xxx}(f_1, f_2) = \lim_{T\to\infty} \frac{1}{T} E[X_T(f_1 + f_2)X_T^*(f_1)X_T^*(f_2)] \tag{2.20}$$

The auto-bispectrum is a function of two frequency components, f_1 and f_2, which could take on both positive and negative values. The symmetry properties and domain of calculation of the auto-bispectrum are discussed more in the next section. When considering the expected value, the auto-bispectrum would have a small value if the phase of $X_T(f_1 + f_2)X_T^*(f_1)X_T^*(f_2)$ i.e. $\phi(f_1 + f_2) - \phi(f_1) - \phi(f_2)$ varies over the different realizations. On the other hand, it would have a large value if this phase does not vary, which is an indication of quadratic coupling between f_1 and f_2

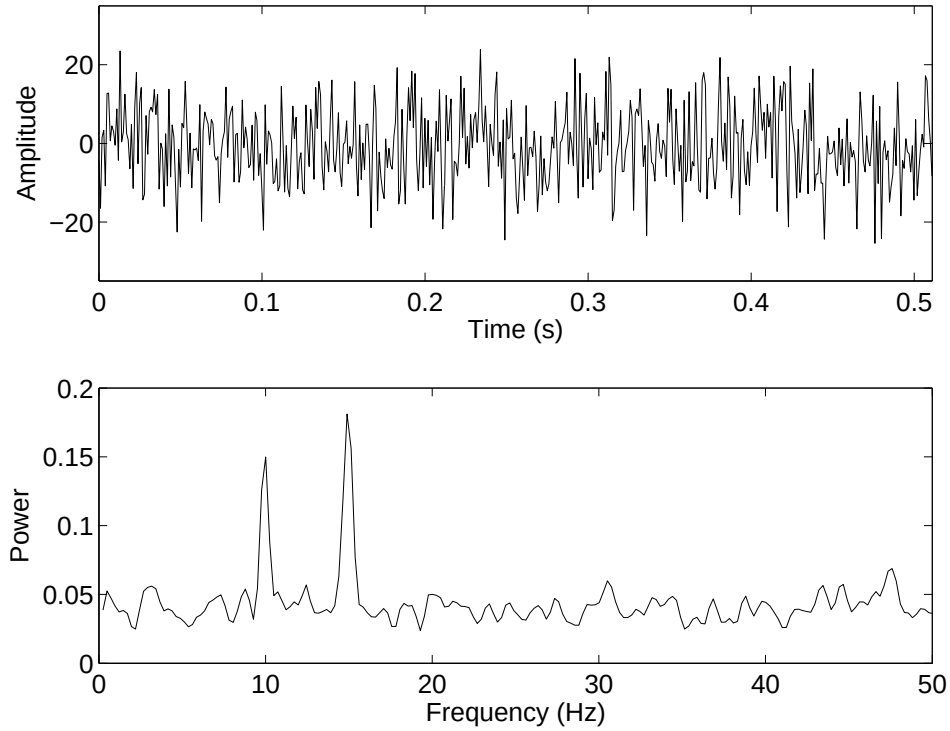

Figure 2.2: A portion of a time series consisting of a $10Hz$ sinusoid, a $15Hz$ sinusoid, and additive white Gaussian noise is shown in the top of the figure. The power spectrum is shown in the bottom of the figure.

[18].

Auto-Bicoherence

The normalized auto-bispectrum, namely the auto-bicoherence, which is defined as [18]

$$b^2_{xxx}(f_1, f_2) = \lim_{T\to\infty} \frac{1}{T} \frac{|B_{xxx}(f_1, f_2)|^2}{E[|X_T(f_1 + f_2)|^2]E[X_T(f_1)X^*_T(f_1)]E[X_T(f_2)X^*_T(f_2)]} \tag{2.21}$$

is limited to values between zero and one. Thus, it is more useful than the auto-bispectrum for assessment of the degree of quadratic coupling. A value of one indicates perfect quadratic phase coupling at the frequency triple (f_1, f_2, f_1+f_2) and a value of zero indicates the absence of quadratic phase coupling. Partial coupling is indicated if the value is in between. This may be the case if the coupling is corrupted by noise. The auto-bicoherence of a signal containing frequencies at $7Hz$ and $10Hz$ and phase coupled content at $17Hz$ and $3Hz$, sampled at a frequency $f_s = 100Hz$, is illustrated in Figure 2.4. A region larger than the full $2-D$ domain is represented by the f_1-f_2 axes,

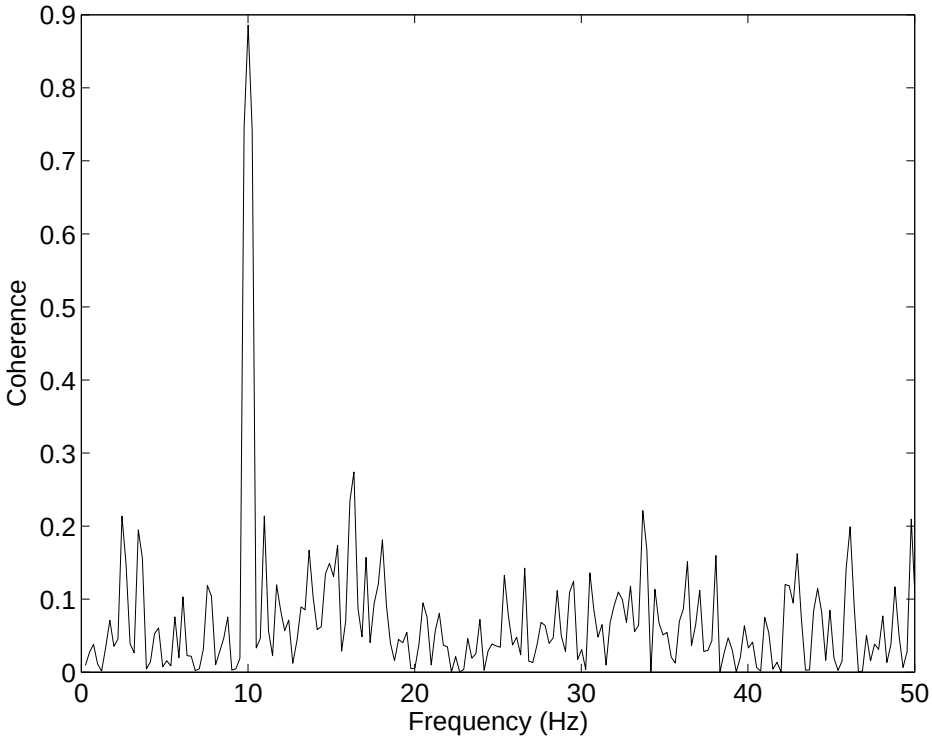

Figure 2.3: Linear coherence between a signal containing one 10Hz sinusoid and a signal containing one phase coupled 10Hz sinusoid, 20Hz sinusoid and random noise.

where the negative values of f_i represent a frequency difference rather than a frequency summation. The z-axis represents the sum $f_1 + f_2$ and the color represents the value of the auto-bicoherence at a particular triple of frequencies.

The bicoherence is typically projected onto the f_1-f_2 plane and displayed as a contour plot as shown in Figure 2.5. The computational domain of the auto-bispectrum and auto-bicoherence can be diminished by making use of the symmetry properties, e.g.,

$$b^2_{xxx}(f_1, f_2) = b^2_{xxx}(f_2, f_1) \tag{2.22}$$

The conditions on f_1 are limited by the Nyquist frequency as, $f_N 0 \leq f_1 \leq f_N$, and the conditions on f_2 are $f_1 \leq f_1 + f_2 \leq f_N$ as indicated in the figure. Quadratic coupling is indicated at twenty four points in the domain, however, only two points, $(3Hz, 7Hz, 10Hz)$ and $(10Hz, 7Hz, 17Hz)$ represent unique sets of coupled frequencies. All other points are redundant and those related to $(3Hz, 7Hz, 10Hz)$ are indicated with a "□", and those related to $(10Hz, 7Hz, 17Hz)$ are indicated with a "◯". In order to speed computation, the domain is limited to the non-redundant region,

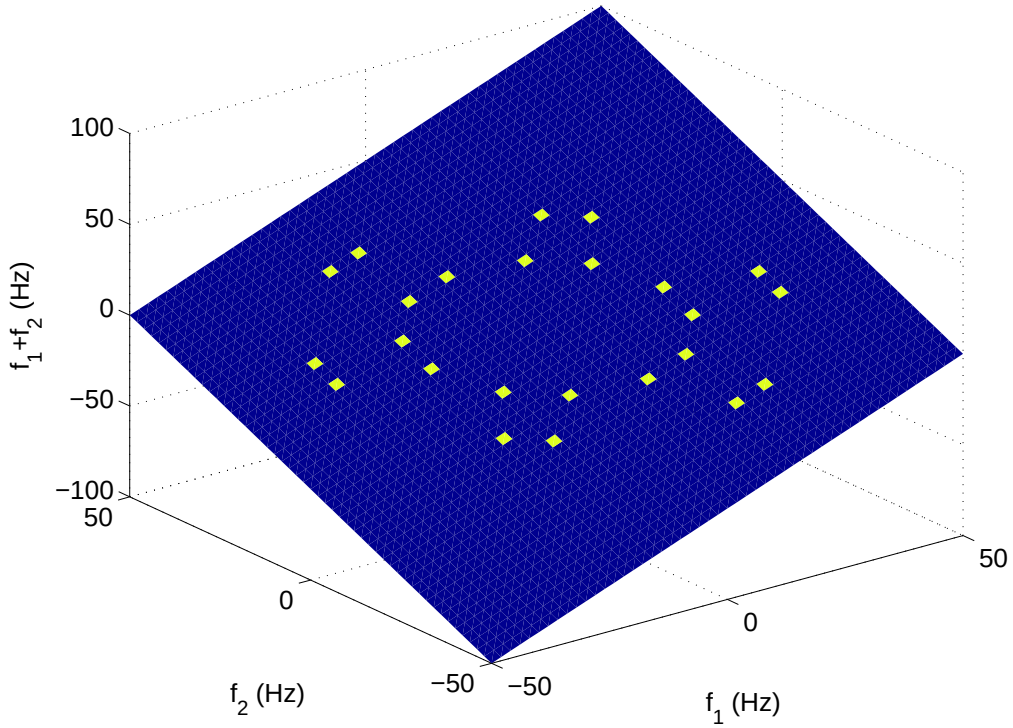

Figure 2.4: Full domain and range of the auto bicoherence. A large amplitude (lighter color) indicates phase coupling of f_1, f_2, and $f_1 + f_2$.

referred to as the "principle domain", as marked by the black triangle [18].

The final form of the auto-bicoherence is shown in Figure 2.6. Quadratically phase coupled frequency triples are indicated at $(3Hz, 7Hz, 10Hz)$ and $(10Hz, 7Hz, 17Hz)$ indicated by a "□" and "◯" respectively, and no other redundant points are shown.

Cross-Bispectrum

Following the definition of the auto-bispectrum, the cross-bispectrum is used to determine the quadratic coupling between frequency components in two different signals. Considering two signals whose Fourier transforms are given by $X(f)$ and $Y(f)$, the cross-bispectrum is defined by [18]

$$B_{yxx}(f_1, f_2) = \lim_{T\to\infty} \frac{1}{T} E[Y_T(f_1 + f_2) X_T^*(f_1) X_T^*(f_2)] \tag{2.23}$$

Through this definition, the coupling level between two frequency components in $X(f)$ namely f_1 and f_2 and their algebraic sum in $Y(f)$ is determined. Again, this is based on the phase relation between these components in the different realizations used in determining the expected value.

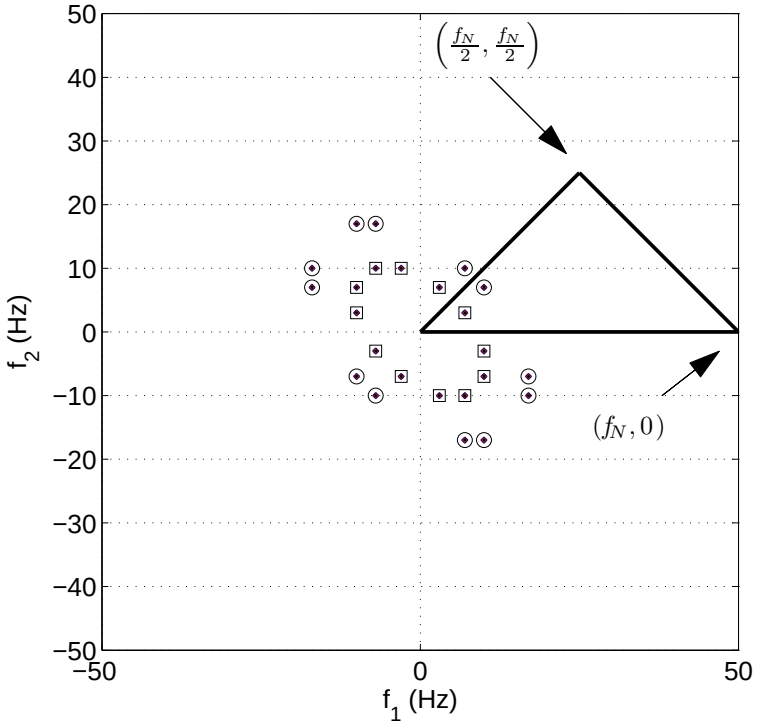

Figure 2.5: Projection of the auto-bicoherence on the f_1-f_2 plane, with the principal domain indicated.

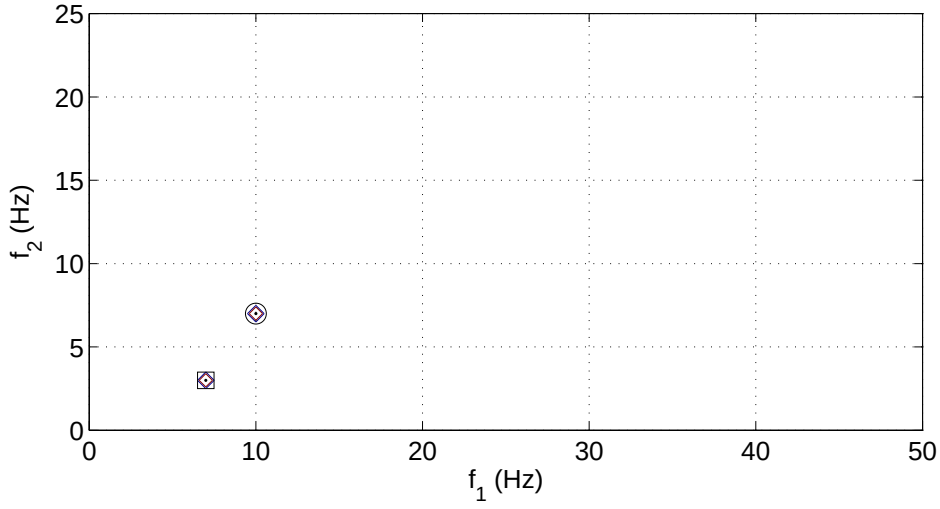

Figure 2.6: Auto bicoherence calculated over the principle domain.

A large value of the cross-bispectrum indicates high quadratic phase coupling between $X(f)$ and $Y(f)$.

Cross-Bicoherence

Following the convention introduced with the auto-bispectrum, the cross-bispectrum is often normalized to yield the cross-bicoherence. The cross-bicoherence is defined as [18]

$$b^2_{yxx}(f_1, f_2) = \lim_{T\to\infty} \frac{1}{T} \frac{|B_{yxx}(f_1, f_2)|^2}{E[|Y_T(f_1 + f_2)|^2]E[|X_T(f_1)|^2]E[|X_T(f_2)|^2]} \tag{2.24}$$

Based on Schwarz's inequality, the value of the cross-bicoherence is bounded between $[0, 1]$. A value of cross-bicoherence close to one indicates strong quadratic phase coupling and a value near zero indicates the absence of coupling.

The cross-bicoherence of a system where the input contains $7Hz$ and $10Hz$ sinusoids and the output contains phase coupled $7Hz$, $10Hz$, $3Hz$, and $17Hz$ sinusoids (and noise) is shown in Figure 2.7*a*. The cross-bicoherence has fewer symmetries than the auto-bicoherence so a larger principle domain is admitted as indicated by the marked region. The two points $(10Hz, -7Hz, 3Hz)$ indicated by a "□" and $(10Hz, 7Hz, 17Hz)$ indicated by a "◯" represent the only two unique sets of frequencies. All other related points are marked with a similar symbol. The expanded domain includes negative frequencies which represent frequency differencing. The conditions on f_1 are $0 \leq f_1$, and the conditions on f_2 are $0 \leq f_1 + f_2 \leq f_N$. The final presentation of the cross-bicoherence is shown in Figure 2.7*b*. The two points shown indicate the phase coupled sum and difference of the input frequencies.

Auto-Trispectrum

The next higher order spectral moment to the bispectrum is the trispectrum. The auto-trispectrum is defined as

$$S_{xxxx}(f_1, f_2, f_3) = \lim_{T\to\infty} \frac{1}{T} |E[X_T(f_1 + f_2 + f_3)X^*_T(f_1)X^*_T(f_2)X^*_T(f_3)]| \tag{2.25}$$

Based on this definition, the trispectrum will give a large value if the phase relation between $X_T(f_1 + f_2 + f_3)X^*_T(f_1)X^*_T(f_2)X^*_T(f_3)$ is constant over the different realizations. A large value of

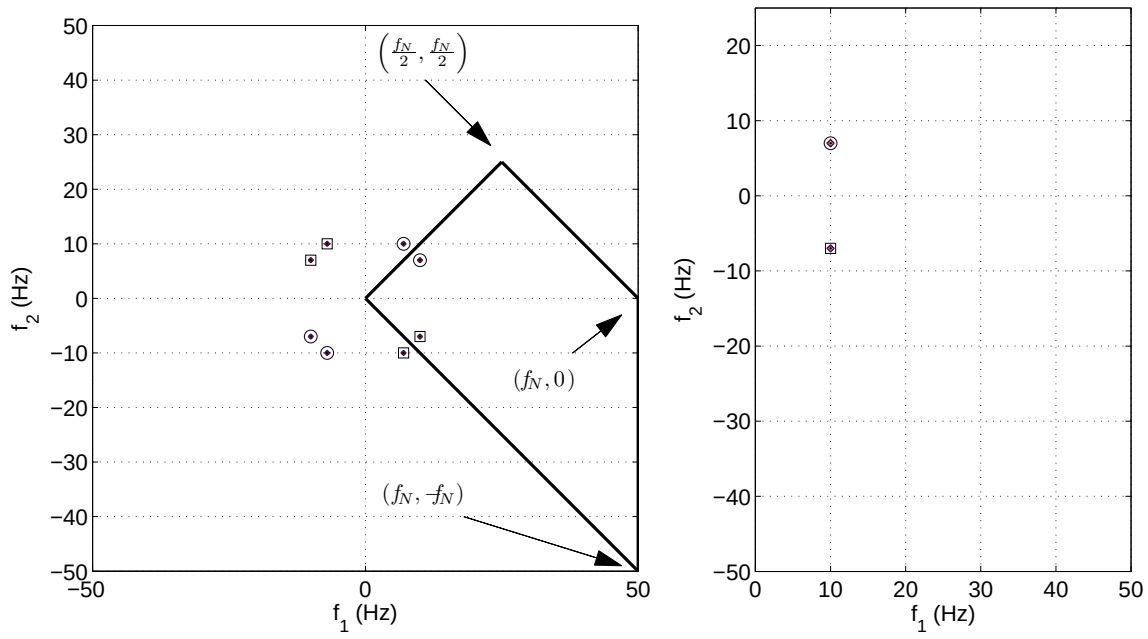

(a) (b)

Figure 2.7: The full domain of the cross-bicoherence of a quadratic system with the principle domain indicated (a), and the final form of the cross-bicoherence of the same system (b)

the trispectrum indicates the presence of a cubic nonlinearity.

Auto-Tricoherence

The normalized auto-trispectrum is referred to as the auto-tricoherence, which is defined as [18]

$$s^2_{xxxx}(f_1, f_2, f_3) = \lim_{T\to\infty} \frac{1}{T} \frac{S^2_{xxxx}(f_1, f_2, f_3)}{E[|X_T(f_1 + f_2 + f_3)|^2]E[|X_T(f_1)|^2]E[|X_T(f_2)|^2]E[|X_T(f_3)|^2]} \tag{2.26}$$

Like the previously defined coherence spectra, the auto-tricoherence is bound between $[0, 1]$. A value of tricoherence close to one indicates strong cubic coupling, while a value between $[0, 1]$ indicates partial cubic coupling.

2.2.4 Numerically Solved Quadratic System

To explain the usefulness of higher order spectra in characterizing quadratic systems, and to show how higher order spectra can be used to identify parameters in nonlinear systems, a quadratic

system of the form

$$\ddot{u}(t) + \omega^2 u(t) + \epsilon\delta u^2(t) = FCos\,(\Omega t + \beta) \tag{2.27}$$

is considered. First, an approximate solution under non-resonance conditions is obtained. The same system is then solved numerically. Results from the approximate solution are matched with higher order spectral analysis of the numerically generated data (with added noise)

The approximate solution is calculated by expanding $u(t) \longrightarrow u_0(t) + \epsilon u_1(t)$. Keeping terms up to $O(\epsilon^1)$ yields,

$$\ddot{u}_0(t) + \epsilon\ddot{u}_1(t) + \omega^2 u_0(t) + \epsilon\omega^2 u_1(t) + \epsilon\delta u_0^2(t) = FCos\,(\Omega t + \beta) \tag{2.28}$$

Collecting powers of ϵ^0 gives

$$\epsilon^0 : \quad \ddot{u}_0(t) + \omega^2 u_0(t) = FCos\,(\Omega t + \beta) \tag{2.29}$$

The general solution to the above equation is given by

$$u_0(t) = Ae^{-i\omega t} + \overline{A}e^{i\omega t} + \Lambda e^{i(\Omega t+\beta)} + \Lambda e^{-i(\Omega t+\beta)} \tag{2.30}$$

where the first set of complex conjugate pairs represents the homogeneous solution, and the second set of complex conjugate pairs represents the particular solution. The constants are defined as

$$A = \frac{c_1}{2} + \frac{ic_2}{2}; \quad \Lambda = \frac{F}{2(\Omega^2 - \omega^2)} \tag{2.31}$$

where c_1 and c_2 depend on the initial conditions. Collecting powers of ϵ^1 gives

$$\epsilon^1 : \quad \ddot{u}_1(t) + \omega^2 u_1(t) = -\delta u_0^2(t) \tag{2.32}$$

The particular solution to this equation is given by

$$u_1(t) = \begin{cases} -\frac{2\delta}{\omega^2}\left(\Lambda^2 + |A|^2\right) + \frac{\delta}{3\omega^2}\left(A^2 e^{2i\omega t} + \overline{A}^2 e^{-2i\omega t}\right) \\ \quad + \frac{\delta\Lambda^2}{4\Omega^2-\omega^2}\left(e^{2i(\Omega t+\beta)} + e^{-2i(\Omega t+\beta)}\right) \\ + \frac{2\delta\Lambda}{\Omega(2\omega+\Omega)}\left(Ae^{i((\Omega+\omega)t+\beta)} + \overline{A}e^{-i((\Omega+\omega)t+\beta)}\right) \\ + \frac{2\delta\Lambda}{\Omega(\Omega-2\omega)}\left(\overline{A}e^{i((\Omega-\omega)t+\beta)} + Ae^{-i((\Omega-\omega)t+\beta)}\right) \end{cases} \tag{2.33}$$

The final approximate solution is given by

$$u(t) = u_0(t) + \epsilon u_1(t) \tag{2.34}$$

In addition to a mean component, the resulting system contains the following frequencies: ω, 2ω, Ω, 2Ω, $\omega+\Omega$ and $\omega-\Omega$. Obviously, the quadratic nonlinearity resulted in the D. C. components and the sum and difference frequency components 2ω, 2Ω, $\omega+\Omega$ and $\omega-\Omega$. Combination resonances occur through small divisor terms if $\Omega = \pm\omega/2$ or $\Omega = \pm 2\omega$, that is, if the system is forced at half or double its natural frequency.

A numerical solution to the full nonlinear system

$$\ddot{u}(t) + \omega^2 u(t) + \epsilon\delta u^2(t) = FCos\left(\Omega t + \beta\right) + \tilde{n}(t) \tag{2.35}$$

with $\omega = 2\pi(4)$, $\epsilon = 1$, $\delta = 40$, $F = 1000$, $\Omega = 2\pi(10)$, $\beta = \pi/8$, and stochastic noise over the interval $[-5.0, 5.0]$ represented by $\tilde{n}(t)$ is presented in Figure 2.8. The spectrum indicates high power at: 4 Hz, 8 Hz, 10 Hz, 20 Hz, 14 Hz, and 6 Hz as expected from the approximate solution in Eq. 2.34.

Quadratic phase coupling is confirmed by calculating the auto-bicoherence of $u(t)$, presented in Figure 2.9 with contour levels at $(0.5 : 0.1 : 0.9)$. Strong quadratic nonlinearities are indicated at lo-

cations representing the doubles $(4Hz, 4Hz, 8Hz)$ and $(10Hz, 10Hz, 20Hz)$, sum $(10Hz, 4Hz, 14Hz)$, and difference $(6Hz, 4Hz, 10Hz)$ frequencies. This confirms $u(t)$ originated from a system with a quadratic nonlinearity. Other peaks, with lower contour values, at $(8Hz, 6Hz, 14Hz)$, $(14Hz, 6Hz, 20Hz)$, represent combination couplings from higher order terms [47]. Obviously, the amplitude and phase of the bispectrum could be used to identify the parameters in the approximate solution, which are, in turn, related to the parameters of the nonlinear system in Eq. 2.27.

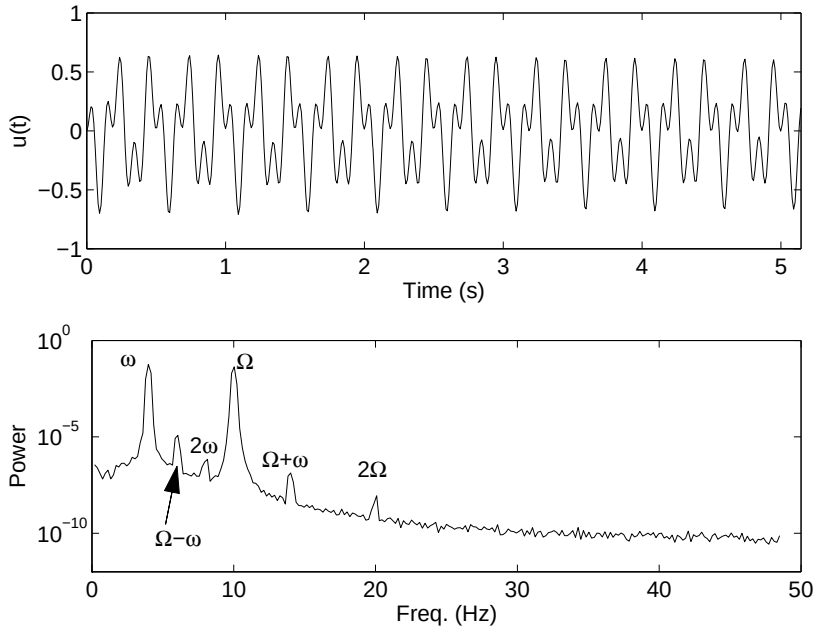

Figure 2.8: Time series (top) and power spectrum (bottom) of the numerically solved quadratic system given in equation 2.35.

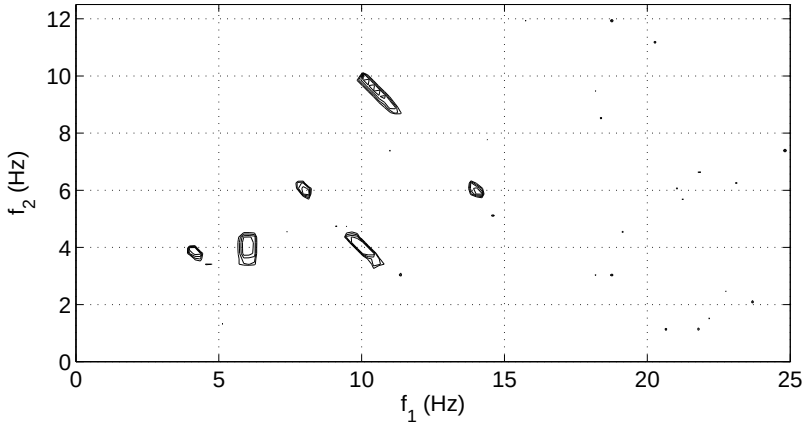

Figure 2.9: Auto-bicoherence of the numerically solved quadratic system given in equation 2.35.

2.2.5 Numerically Solved Cubic System

To show the usefulness of the auto-tricoherence in the identification of cubic nonlinearities, a self excited nondimensional cubic system of the form

$$\ddot{u}(t) + u(t) + \epsilon\alpha u^3(t) = 0 \tag{2.36}$$

is considered. An approximate solution with $u(0) = aCos(\beta)$ and $\dot{u}(0) = -aSin(\beta)$ is obtained, where β is the initial phase. A straightforward expansion is calculated by expanding $u(t) \longrightarrow u_0(t) + \epsilon u_1(t)$ and keeping terms of $O(\epsilon^1)$, which yields

$$\ddot{u}_0(t) + \epsilon\ddot{u}_1(t) + u_0(t) + \epsilon u_1(t) + \epsilon\alpha u_0^3(t) = 0 \tag{2.37}$$

Collecting terms of $O(\epsilon^0)$ gives

$$\epsilon^0 : \quad \ddot{u}_0(t) + u_0(t) = 0 \tag{2.38}$$

The general solution to this equation is given by

$$u_0(t) = aCos(t + \beta) \tag{2.39}$$

Collecting terms of $O(\epsilon^1)$ gives

$$\epsilon^1 : \quad \ddot{u}_1(t) + u_1(t) = -\alpha u_0^3(t) \tag{2.40}$$

The particular solution to this equation is given by

$$u_1(t) = \frac{\alpha a^3}{32}\left(-6Cos\left(t + \beta\right) + Cos\left(3\left(t + \beta\right)\right) - 12tSin\left(t + \beta\right)\right) \tag{2.41}$$

An approximate analytical solution is then written as

$$u(t) = u_0(t) + \epsilon u_1(t) \tag{2.42}$$

A numerical solution to the nondimensional self excited cubic system

$$\ddot{u}(t) + u(t) + \epsilon\alpha u^3(t) = \tilde{n}(t) \tag{2.43}$$

with $\epsilon = 1$, $\alpha = 3$, $u(0) = 1$, $\dot{u}(0) = 1$, and stochastic noise over the interval $[-0.005 - 0.005]$ represented by $\tilde{n}(t)$ is presented in Figure 2.10. The two largest components in the power spectrum are $0.31Hz$ and $0.93Hz$. The natural frequency of the system is increased due to the cubic nonlinearity [47]. The frequency content is consistent with a cubic nonlinearity which is confirmed by the auto-tricoherence calculation, shown in Figure 2.11. The tricoherence is a four dimensional quantity and, as such, it is difficult to visualize. Typically, f_1, f_2, and f_3 are the axes of the cartesian cube and $s^2_{xxxx}(f_1, f_2, f_3)$ is represented as a point of varying size or color in three dimensional space. The auto-tricoherence has ninety six regions of symmetry and the principle domain is a wedge in 3-space as described by Collis et al. [9]. The points are colored according to the value of $s^2_{xxxx}(f_1, f_2, f_3)$ and only the largest tricoherence values are plotted. Projections of $s^2_{xxxx}(f_1, f_2, f_3)$, marked by x's, are shown on three orthogonal planes as well. Although the data are spread, the highest tricoherence values have a frequency sum of $\approx 0.93Hz$.

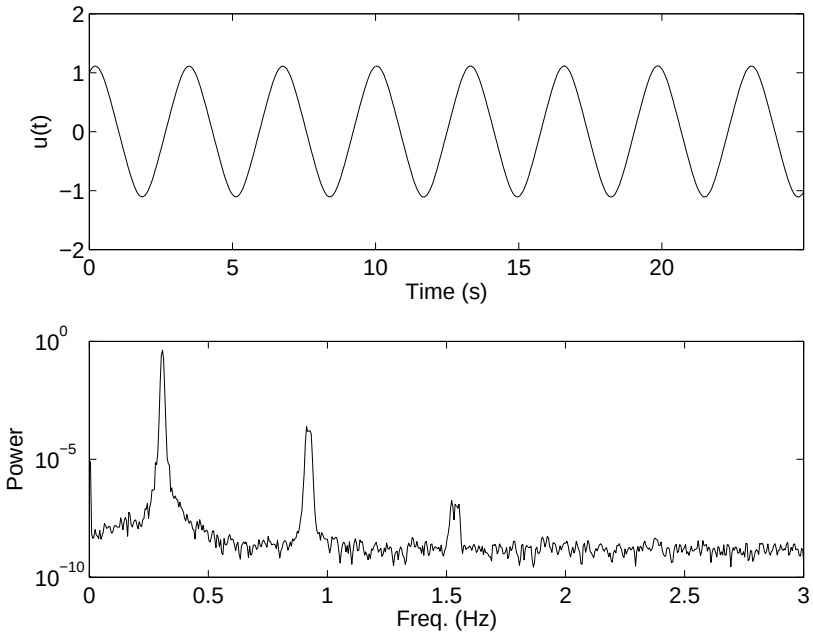

Figure 2.10: Time series (top) and power spectrum (bottom) of the numerically solved cubic system given in equation 2.43.

Below, a new method of visualizing the auto tricoherence is presented in Figure 2.12. The value of tricoherence is plotted on the vertical axis, and frequency is plotted on the horizontal axis. Each of the three frequencies f_1, f_2, and f_3 is indicated by a different symbol. The frequency combinations are represented by a distinct symbol as well. In this case, only the frequency sum is shown as represented by a dot ($\cdot$). The highest values of tricoherence are immediately identified at $\approx 0.93Hz$. A higher harmonic is also present at $\approx 1.5Hz$.

Plotting the tricoherence as such has the following advantages:

- Usually only the largest values of tricoherence are important, these can be read easily and would not be overlapped by other values.
- An arbitrary number of frequency combinations can be represented by using a distinct color for each combination e.g. red for $f_1 + f_2 + f_3$, green for $f_1 + f_2 - f_3$ etc.
- The combination frequency is displayed explicitly. The importance of this is illustrated by comparing Figure 2.10*b* and Figure 2.12. Although both figures show the individual frequencies, f_i, their combinations, Σf_i, are clearly concentrated around $0.93Hz$ and $1.5Hz$ as indicated in Figure 2.12.
- The individual frequency triples can still be identified since relatively few triplets occur at a given level of tricoherence.

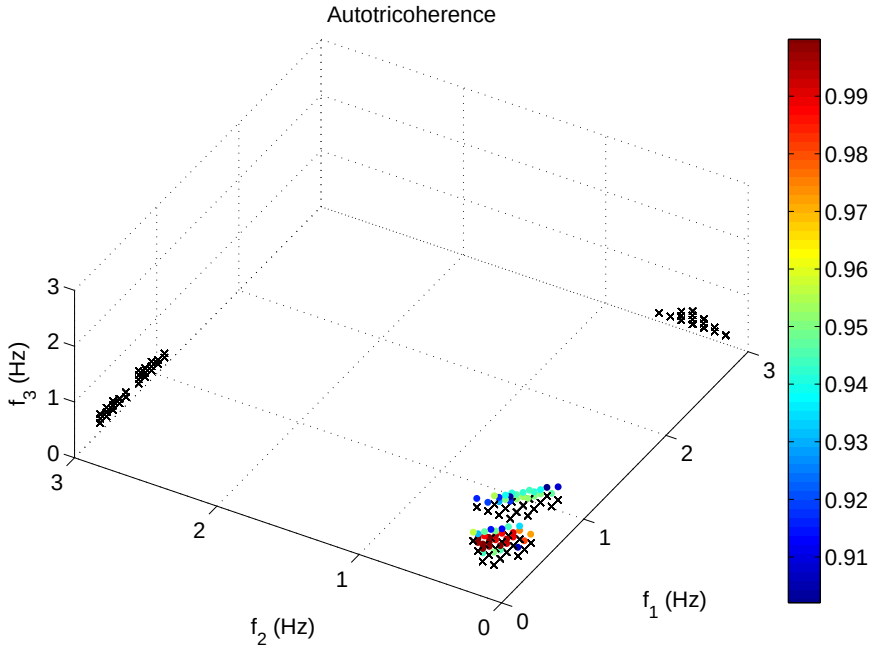

Figure 2.11: Auto-tricoherence of the numerically solved cubic system given in equation 2.43.

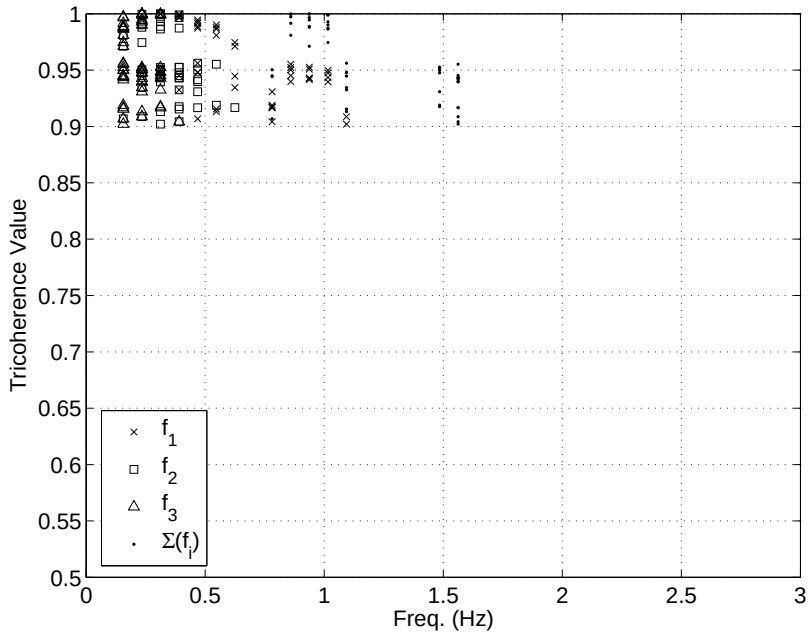

Figure 2.12: The auto-tricoherence plotted in two dimensions using different symbols.

2.3 Wavelet-Based Analysis Tools

In this section, wavelet analysis is introduced. A computer implementation of the continuous wavelet transform is verified, and several advantages for the analysis of nonstationary time series over Fourier-based analysis are discussed. The spectral moments introduced in the previous section are re-written in terms of wavelet coefficients. The advantage of using wavelet-based, rather than Fourier-based, higher order spectra in the identification of an intermittently quadratically coupled system is demonstrated using a numerical example.

2.3.1 Continuous Wavelet Transform

Complex physical systems often exhibit aperiodic, transient or intermittent fluctuations. It is possible that harmonic content will persist for several cycles and then shift, or decay completely, due to saturation or other nonlinear phenomena. Fourier-based analysis is inadequate for such systems because of the requirement for ensemble averaging. Wavelet analysis, on the other hand, allows the characterization of a signal in the frequency and time domains simultaneously. This allows identification of instantaneous frequencies over short time periods.

The continuous wavelet transform, denoted as CWT, is defined as [22]

$$CWT\{x(t)\}(a,\tau) = W(a,\tau) = \int_{-\infty}^{\infty} x(t)\Psi_m^*\left(\frac{t-\tau}{a}\right)dt \tag{2.44}$$

where $x(t)$ is the time series being analyzed, a is the wavelet scale which is proportional to $1/freq$, τ is the wavelet time, and $\Psi_m(t)$ is the mother wavelet. The superscript * represents the complex conjugate operation. Many choices are available for the choice of basis function, referred to as the mother wavelet. This function can be chosen to match the fluctuation characteristics of a particular system. Yet, the wavelet must have zero mean and decay to zero as time goes to infinity [48], which are referred to as the admissability conditions. The equivalent conditions in the frequency domain require that the wavelet has a zero DC component and finite frequency support.

2.3.2 Some Characteristics of the Morlet Wavelet

Morlet Wavelet Definition

The Morlet wavelet, which is a complex sinusoid windowed by a Gaussian function, is the wavelet basis used throughout this work. The Morlet wavelet contains a complex sinusoid which makes it well suited for analyzing harmonic signals. Although the Morlet wavelet does not strictly satisfy the zero mean criteria, the small error that is introduced is insignificant in practical digital implementations [49] and [24]. The mother wavelet is defined as [50]

$$\Psi_m(t) = \frac{1}{\sqrt{\pi F_b}} e^{2i\pi F_c t} e^{\frac{-t^2}{F_b}} \tag{2.45}$$

All other wavelets in the family are scaled and shifted versions of this wavelet which are defined by multiplying by a factor of $1/\sqrt{a}$ and applying the mapping $t \rightarrow \frac{t-\tau}{a}$ giving

$$\Psi(a,t) = \frac{1}{\sqrt{\pi F_b a}} e^{2i\pi F_c (t-\tau)/a} e^{\frac{-((t-\tau)/a)^2}{F_b}} \tag{2.46}$$

The scale parameter, a, acts to scale the wavelet, F_c is the center frequency, and F_b is related to the bandwidth.

Time Domain Properties

Several properties of the scaled Morlet wavelet with $\tau = 0$ are described below. The wavelet magnitude peak occurs at $t = 0$, with a value of

$$|\Psi(a,0)| = \frac{1}{\sqrt{aF_b\pi}} \tag{2.47}$$

The characteristic decay time, D_t, is calculated based on the definition given by [51] as

$$D_t = \sqrt{\frac{\int_{-\infty}^{\infty} t^2 \left|\Psi(a,t)\right|^2 dt}{\int_{-\infty}^{\infty} \left|\Psi(a,t)\right|^2 dt}} = a\frac{\sqrt{F_b}}{2} \tag{2.48}$$

The decay time gives insight into the temporal support of the wavelet. The value one D_t away from the peak is given by

$$\left|\Psi\left(a, a\frac{\sqrt{F_b}}{2}\right)\right| = \frac{1}{e^{1/4}\sqrt{aF_b\pi}} \tag{2.49}$$

An increase in the value of F_b acts to increase the temporal support of the wavelet, as does an increase in the scale parameter, a.

Frequency Domain Properties

The Fourier transform of the Morlet wavelet gives insight into the frequency response of the wavelet. Carrying out the operation as defined in Equation 2.9 yields

$$\hat{\Psi}(a, f) = \sqrt{a}e^{-F_b\pi^2(af-F_c)^2} \tag{2.50}$$

where the $\hat{}$ denotes the Fourier domain. The result is a Gaussian function that is purely real. Note that the wavelet has localized support in the frequency domain [52]. The frequency of peak response of the wavelet is commonly referred to as the wavelet's frequency [53] even though the wavelet contains a distribution of frequencies. By setting the argument of the exponential term equal to zero, the frequency of largest response is calculated as

$$f = \frac{F_c}{a} \tag{2.51}$$

Therefore, a wavelet with scale, a, has an equivalent frequency of F_c/a. The value at the peak frequency is

$$\hat{\Psi}\left(a, \frac{F_c}{a}\right) = \sqrt{a} \tag{2.52}$$

A measure of the frequency support, D_f, centered at the peak frequency is calculated as

$$D_f = \sqrt{\frac{\int_{-\infty}^{\infty}(f-(F_c/a))^2\left|\hat{\Psi}(a,f)\right|^2 df}{\int_{-\infty}^{\infty}\left|\hat{\Psi}(a,f)\right|^2 df}} = \frac{1}{2a\pi\sqrt{F_b}} \tag{2.53}$$

An increase in the bandwidth parameter, F_b, acts to decrease the frequency support, as does an

increase in the scale parameter a. An increase in the center frequency, F_c, increases the peak frequency but does not affect the frequency support. The value one D_f away from the peak is

$$\hat{\Psi}\left(a, \frac{1}{2a\pi 2\sqrt{F_b}}\right) = \frac{\sqrt{a}}{e^{1/4}} \tag{2.54}$$

A comparison of the time domain and frequency domain properties of the Morlet wavelet is presented in Figure 2.13, which summarizes the above results.

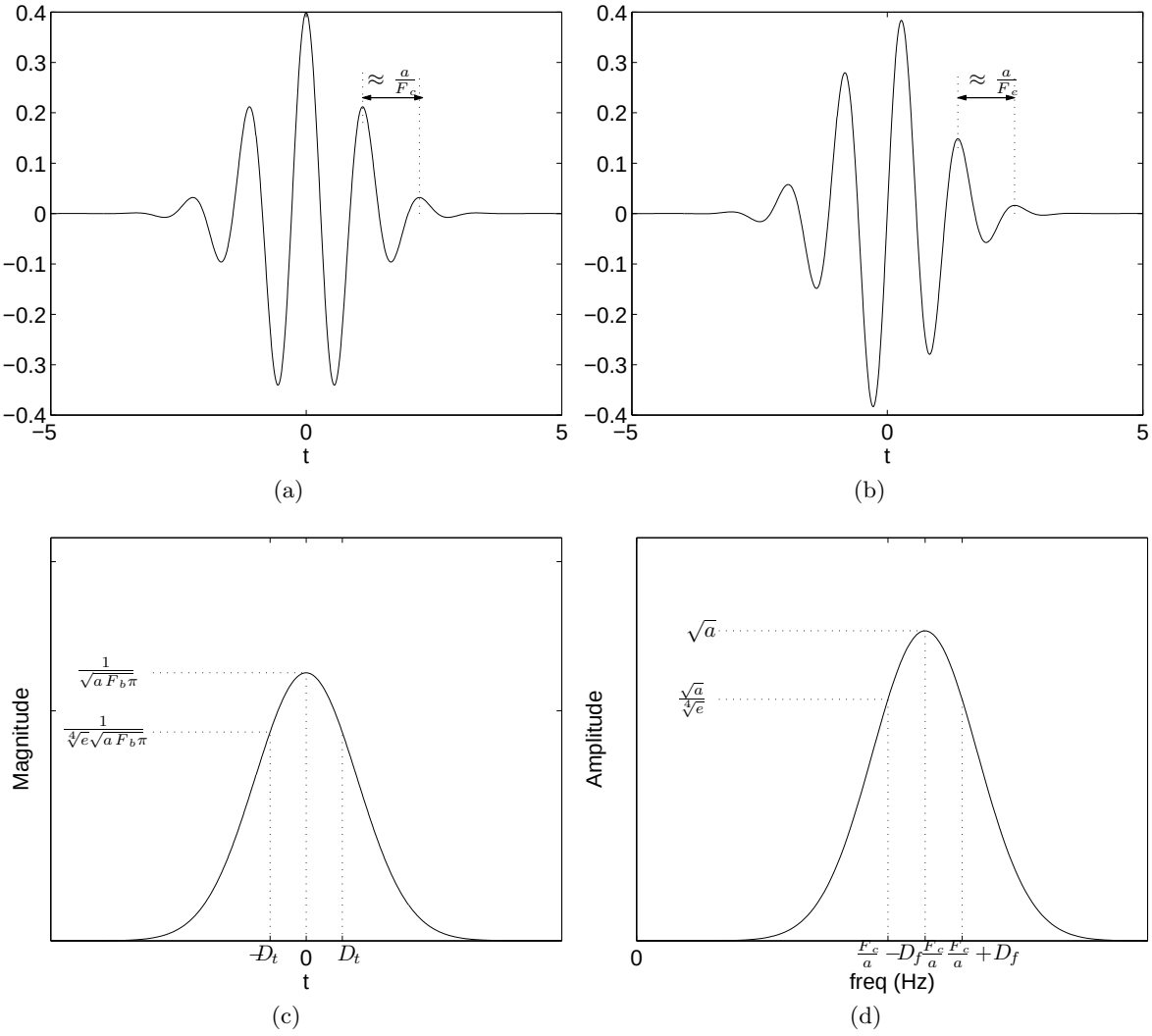

Figure 2.13: The real part (a), imaginary part (b), magnitude (c), and Fourier domain (d) of a Morlet wavelet with $\tau = 0$.

Energy

The energy of a signal can be calculated in the frequency domain as well as in the time domain [17]. This equivalence is expressed as Parseval's Theorem and is shown as

$$E = \int_{-\infty}^{\infty} |x(t)|^2 dt = \int_{-\infty}^{\infty} |X(f)|^2 df \tag{2.55}$$

Since the Morlet wavelet is a complex sinusoid windowed by a Gaussian, the magnitude $|\Psi(a,t)|$ is simply the magnitude of the Gaussian, and the energy of the scaled wavelet is calculated as

$$E = \int_{-\infty}^{\infty} \frac{1}{\pi F_b a} e^{\frac{-2(t/a)^2}{Fb}} dt = \frac{1}{\sqrt{2\pi F_b}} \tag{2.56}$$

Note that the energy is independent of the scale, a.

2.3.3 Frequency Domain Implementation

The continuous wavelet transform is a cross correlation between the time series and the scaled wavelet functions. Under special circumstances, the cross correlation between two functions is equivalent to a convolution operation, denoted by $f * g$, shown as

$$f * g = \int_{-\infty}^{\infty} g(t) f(\tau - t) dt \tag{2.57}$$

Efficient numerical implementation can be realized by treating the CWT as a convolution operation. Both speed and accuracy gains are realized since convolution is simply a multiplication in the frequency domain [24]. The equivalence of the cross correlation to the convolution for this specific choice of wavelet is shown below. The definition of the wavelet transform for the scaled and shifted Morlet wavelet is

$$W(a,\tau) = \frac{1}{\sqrt{a}} \int_{-\infty}^{\infty} x(t) \frac{1}{\sqrt{\pi F_b}} e^{-2i\pi F_c\left(\frac{t-\tau}{a}\right)} e^{\frac{-\left(\frac{t-\tau}{a}\right)^2}{F_b}} dt \tag{2.58}$$

Rewriting the equation yields

$$W(a,\tau) = \frac{1}{\sqrt{a}} \int_{-\infty}^{\infty} x(t) \frac{1}{\sqrt{\pi F_b}} e^{2i\pi F_c\left(\frac{\tau-t}{a}\right)} e^{\frac{-\left(\frac{\tau-t}{a}\right)^2}{F_b}} dt \tag{2.59}$$

Noting that the Fourier transform of the Morlet wavelet is

$$F\left\{\Psi\left(a,f\right)\right\} = ae^{-F_b\pi^2(af-F_c)^2} \tag{2.60}$$

The transformed wavelet with its inverse Fourier transform is substituted into the equation to get

$$W(a,\tau) = \sqrt{a}\int_{-\infty}^{\infty} x(t)\left[\int_{-\infty}^{\infty} e^{-F_b\pi^2(af-F_c)^2}e^{2\pi if(\tau-t)}df\right]dt \tag{2.61}$$

Interchanging the order of integration gives

$$W(a,\tau) = \sqrt{a}\int_{-\infty}^{\infty} e^{-F_b\pi^2(af-F_c)^2}\left[\int_{-\infty}^{\infty} x(t)e^{-2\pi ift}dt\right]e^{2\pi if\tau}df \tag{2.62}$$

Further simplification yields

$$W(a,\tau) = \sqrt{a}\int_{-\infty}^{\infty} e^{-F_b\pi^2(af-F_c)^2}F\{x(t)\}e^{2\pi if\tau}df \tag{2.63}$$

Finally, the multiplication in the frequency domain is shown as

$$W(a,\tau) = \sqrt{a}F^{-1}\left\{e^{-F_b\pi^2(af-F_c)^2}F\{x(t)\}\right\} \tag{2.64}$$

2.3.4 Analytical Wavelet Transforms

A computer algorithm was implemented to calculate the continuous wavelet transform used in analyses presented in the subsequent chapters of this work. A comparison between analytically generated results and numerically generated results is used to verify the computer algorithm.

Wavelet Transform of a Delta Function

The wavelet transform of the Dirac Delta function

$$W(a,\tau) = \frac{1}{\sqrt{\pi F_b a}}\int_{-\infty}^{\infty}\delta(t-t_0)e^{2i\pi F_c\left(\frac{\tau-t}{a}\right)}e^{\frac{-\left(\frac{\tau-t}{a}\right)^2}{F_b}}dt \tag{2.65}$$

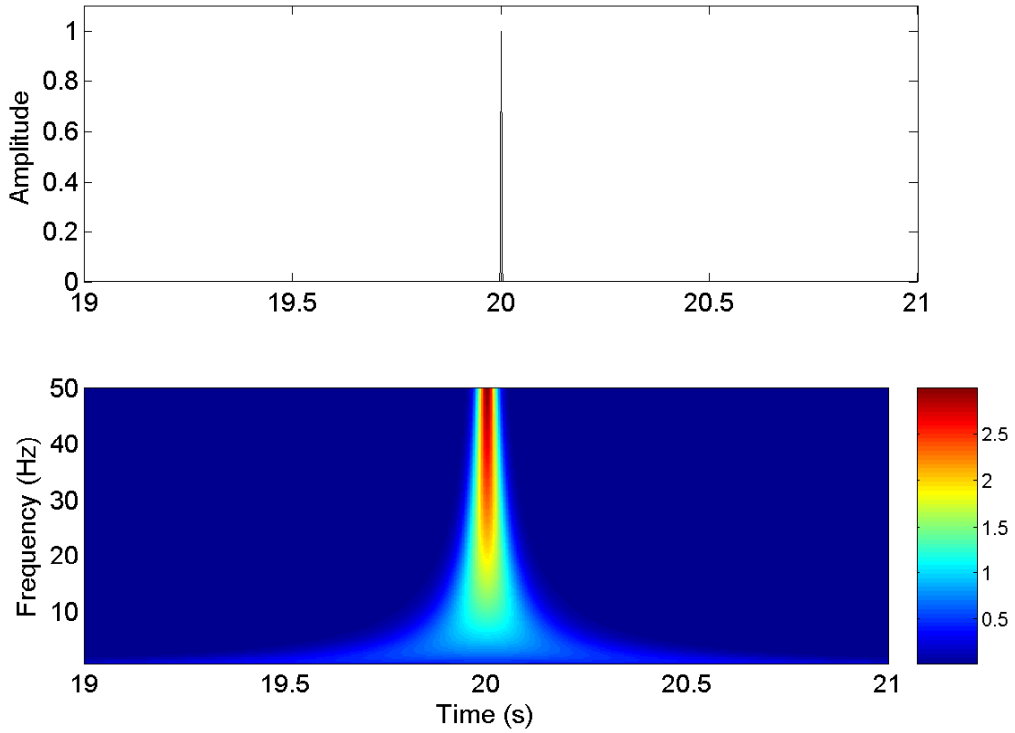

Figure 2.14: Time series (top), and wavelet transform magnitude (bottom), of a delta function.

gives the complex conjugate of the scaled wavelet centered at the time of the delta function. Calculated as

$$W(a,\tau) = \frac{1}{\sqrt{\pi F_b a}} e^{2i\pi F_c\left(\frac{\tau - t_0}{a}\right)} e^{\frac{-\left(\frac{\tau - t_0}{a}\right)^2}{F_b}} \tag{2.66}$$

Choosing $t_0 = 20, F_b = 2, F_c = 0.8753$, and scales a so that the frequency range is $f = [1Hz - 50Hz]$, the magnitude of the resulting wavelet transform is shown in Figure 2.14. Time is displayed on the x-axis, frequency is displayed on the y-axis, and the color represents the magnitude of the wavelet coefficients according to the colorbar. Notice how the wavelet coefficients are distributed in time at the lower frequencies, and more localized in time at higher frequencies. Additionally, the coefficients are localized in frequency at the lower frequencies distributed in frequency at higher frequencies.

A comparison between the real part of the analytical results and the real part of the numerically generated results is shown in Figure 2.15. Two lines are plotted in the figure and an expanded view of certain features are shown. There is good agrement between the analytical results and the numerical implementation.

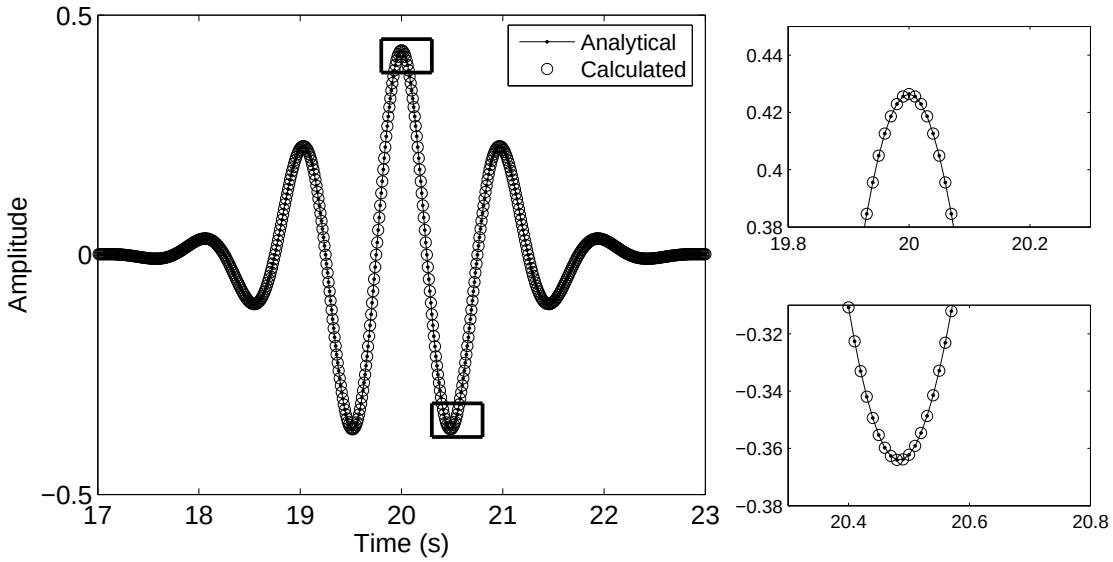

Figure 2.15: Analytical and numerical wavelet transform (real part) of a delta function, $a = 0.8753$. The numerical method gives the same result as the analytical method.

A similar comparison between the imaginary part of the analytical results and the numerically generated results is shown in Figure 2.16. Again, the analytical and numerical results display good agreement.

Wavelet Transform of a Sinusoid

The frequency support of the Morlet wavelet can be demonstrated by taking the wavelet transform of a pure sinusoid. The function, $sin(2\pi f_o t)$, is chosen as an input

$$W(a,\tau) = \frac{1}{\sqrt{\pi F_b a}} \int_{-\infty}^{\infty} sin(2\pi f_o t) e^{2i\pi F_c\left(\frac{\tau - t}{a}\right)} e^{\frac{-\left(\frac{\tau - t}{a}\right)^2}{F_b}} dt \tag{2.67}$$

and the wavelet transform is calculated as

$$W(a,\tau) = i\sqrt{a} e^{-F_b(F_c^2 + a^2 f_o^2)\pi^2} sinh(i2f_0\pi\tau + 2f_0\pi^2 a F_b F_c) \tag{2.68}$$

The resulting function does not vary with τ and has finite frequency support as indicated by the exponential term. This term decays with a^2 as the scale a becomes different from the equivalent scale of the sinusoid. The complex argument in the hyperbolic sine function results in increasing oscillations which are attenuated by the decaying exponential.

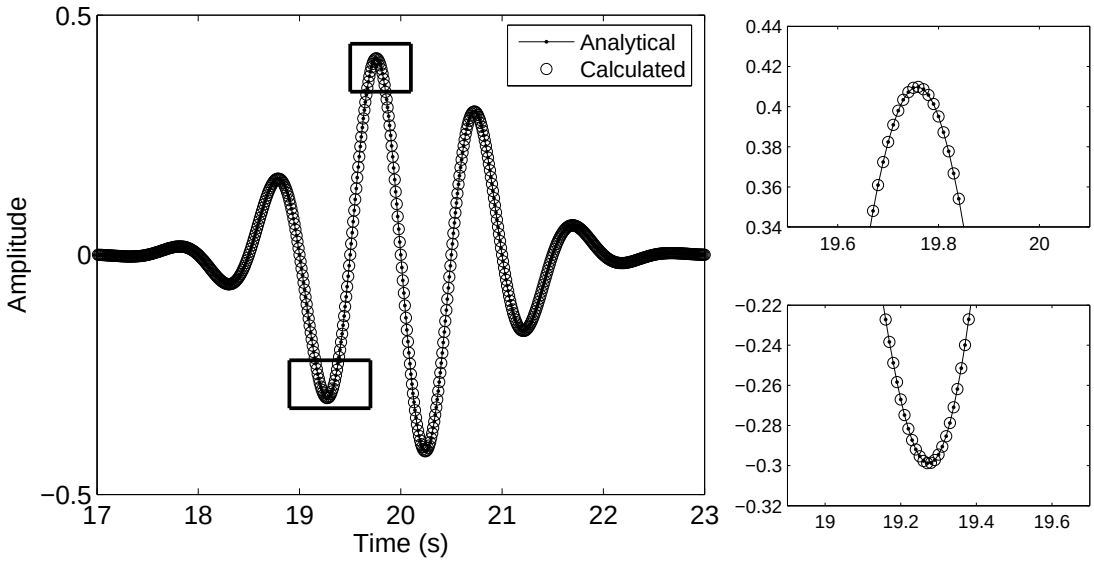

Figure 2.16: Analytical and numerical wavelet transform (imaginary part) of a delta function, $a = 0.8753$. The numerical method gives the same result as the analytical method.

2.3.5 Time/Frequency Characterization

Simultaneous time/frequency characterization is demonstrated by identifying the instantaneous frequency of a chirp signal. A portion of the chirp signal, which ranges in frequency from $5Hz$ to $40Hz$, is shown in the top of the Figure 2.17. The Wavelet Energy Spectrum (WES) defined as [22]

$$WES(a,\tau) = \frac{W(a,\tau)W(a,\tau)^*}{a} \tag{2.69}$$

is shown below. The WES is used as a normalization for purely sinusoidal signals giving a uniform peak throughout the entire frequency range [53]. The instantaneous frequency is correctly identified by the red color (largest magnitude), from $[5Hz - 40Hz]$.

2.3.6 Wavelet-Based Spectral Moments

The spectral moments described in Section 2.2.3 can be expressed in terms of wavelet coefficients. In contrast to the Fourier-based spectral moments, which require many averages over the entire signal interval, the wavelet-based spectral moments can be implemented over a localized time interval. This has the advantage of identifying intermittent harmonic coupling that may be lost if a longer integration time was required.

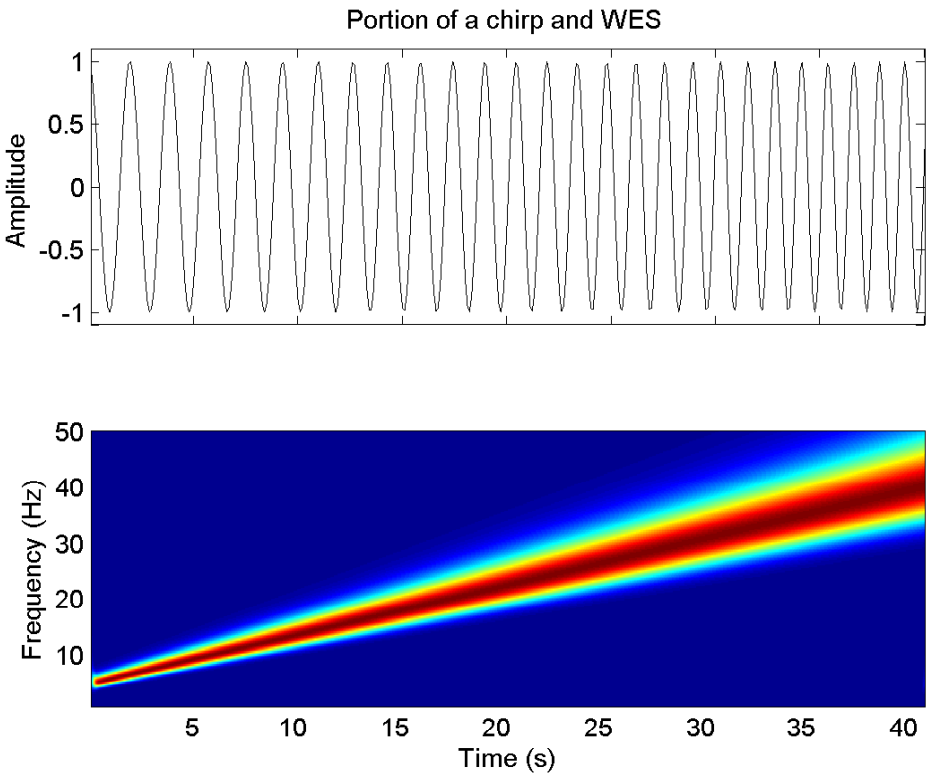

Figure 2.17: Time series (top), and Wavelet Energy Spectrum (bottom), of a chirp.

Wavelet-Based Auto Power Spectrum

The wavelet-based power spectrum is calculated from the wavelet coefficients as [28]

$$P_{xx}^{w}(a) = \int_{T} W_x^*(a,\tau) W_x(a,\tau) d\tau \tag{2.70}$$

Where the integration time, T, represents the interval of interest.

Wavelet-Based Linear Coherence

The wavelet-based linear coherence is defined as [28]

$$[\gamma_{xy}^{w}(a)]^2 = \frac{\left|\int_T W_x^*(a,\tau) W_y(a,\tau) d\tau\right|^2}{P_{xx}^{w}(a) P_{yy}^{w}(a)} \tag{2.71}$$

Wavelet-Based Auto-Bispectrum

The wavelet-based auto-bispectrum is similarly expressed in terms of wavelet coefficients. The frequency summing rule for the addition of scales is $\frac{1}{a} = \frac{1}{a_1} + \frac{1}{a_2}$. The auto-bispectrum is calculated as [28]

$$B^w_{xxx}(a_1, a_2) = \int_T W^*_x(a, \tau) W_x(a_1, \tau) W_x(a_2, \tau) d\tau \tag{2.72}$$

Similar to the Fourier-based auto-bispectrum, the wavelet-based auto-bispectrum is typically normalized to give the wavelet-based auto-bicoherence which is easier to work with.

Wavelet-Based Auto-Bicoherence

The wavelet-based auto-bicoherence is defined as [28]

$$[b^w_{xxx}(a_1, a_2)]^2 = \frac{|B^w_{xxx}(a_1, a_2)|^2}{(\int_T |W_x(a_1, \tau) W_x(a_2, \tau)|^2 d\tau)(\int_T |W_x(a, \tau)|^2 d\tau)} \tag{2.73}$$

The domain and range of this spectral moment are the same as its Fourier counterpart.

Wavelet-Based Cross-Bispectrum

The wavelet-based cross-bispectrum is defined as [28]

$$B^w_{yxx}(a_1, a_2) = \int_T W^*_y(a, \tau) W_x(a_1, \tau) W_x(a_2, \tau) d\tau \tag{2.74}$$

The wavelet-based cross-bispectrum is typically normalized to give the wavelet-based cross-bicoherence.

Wavelet-Based Cross-Bicoherence

The wavelet-based cross-bicoherence is defined as [28]

$$[b^w_{yxx}(a_1, a_2)]^2 = \frac{|B^w_{yxx}(a_1, a_2)|^2}{(\int_T |W_x(a_1, \tau) W_x(a_2, \tau)|^2 d\tau)(\int_T |W_y(a, \tau)|^2 d\tau)} \tag{2.75}$$

The domain and range of this spectral moment are the same as its Fourier counterpart.

Statistical Error of Wavelet-Based HOS

Since the scales of the Morlet wavelet are not orthogonal, some statistical noise is introduced in calculating the spectral moments. Van Milligen et al. estimated the noise level for the wavelet-based linear coherence as [54]

$$\epsilon[\gamma_{xy}^{w}(f)] \approx 2 \left(\frac{F_s}{f}\frac{1}{N}\right)^{1/2} \tag{2.76}$$

and for the wavelet-based bicoherence as [28]

$$\epsilon[b^{w}(f_1, f_2)] \approx \left(\frac{F_s/2}{min(|f_1|, |f_2|, |f_1 + f_2|)}\frac{1}{N}\right)^{1/2} \tag{2.77}$$

At low frequencies, the noise may dominate the results. This can be mitigated by expanding the integration window. However, expanding the integration window may detract from the localized nature of the behavior that is begin analyzed [28]. Only results that are above the noise level are shown in this work.

2.3.7 Wavelet-Bicoherence of an Intermittently Coupled System

The following example illustrates the localized nature of the wavelet-based cross-bicoherence. A system with an input, $x(t)$, and an output, $y(t)$, as defined below, is analyzed with both the Fourier-based cross-bicoherence and the wavelet-based cross-bicoherence. The input/ouput system exhibits uncoupled, partially coupled, and fully coupled behaviors over defined time periods. The time series of the input, shown in the top portion of Figure 2.18a, is defined by

$$x(t) = \begin{cases} Cos(2\pi 10t + \phi_1) + Cos(2\pi 15t + \phi_2) + Cos(2\pi 25t + \phi_3) + n(t), & \text{if } 0 < t < 3 \\ 0, & \text{if } 3 \leq t < 6 \\ Cos(2\pi 10t + \phi_1) + Cos(2\pi 15t + \phi_2) + Cos(2\pi 25t + \phi_3) + n(t), & \text{if } t \geq 6 \end{cases} \tag{2.78}$$

Notice that the input signal contains a 10Hz, a 15Hz and their sum, a $25Hz$ signal. However, the $25Hz$ signal is not phase-coupled to the 10Hz and 15Hz signals. The output, $y(t)$, shown in the bottom portion of Figure 2.18a, is defined by

$$y(t) = \begin{cases} Cos(2\pi 10t + \phi_1) + Cos(2\pi 15t + \phi_2) + & \text{if } 0 < t < 6 \\ (Cos(2\pi 10t + \phi_1) * Cos(2\pi 15t + \phi_2)) + n(t), & \\ 0, & \text{if } 6 \leq t < 8 \\ Cos(2\pi 10t + \phi_1) + Cos(2\pi 15t + \phi_2) + & \\ (Cos(2\pi 10t + \phi_1) * Cos(2\pi 15t + \phi_2)) + n(t), & \text{if } t \geq 8 \end{cases} \tag{2.79}$$

The output, $y(t)$, consists of a $10Hz$, $15Hz$, $25Hz$, and $5Hz$ component. In this case, the $25Hz$ (sum) and the $5Hz$ (difference) components are phase coupled to the $10Hz$ and $15Hz$ components. Since the coupling is intermittent, the Fourier-based cross-bicoherence is an inappropriate tool to identify the coupling. The result of the Fourier-based cross-bicoherence, shown with contours at $(0.5 : 0.1 : 0.9)$ in Figure 2.18*b*, shows partial coupling of the system throughout as would be expected.

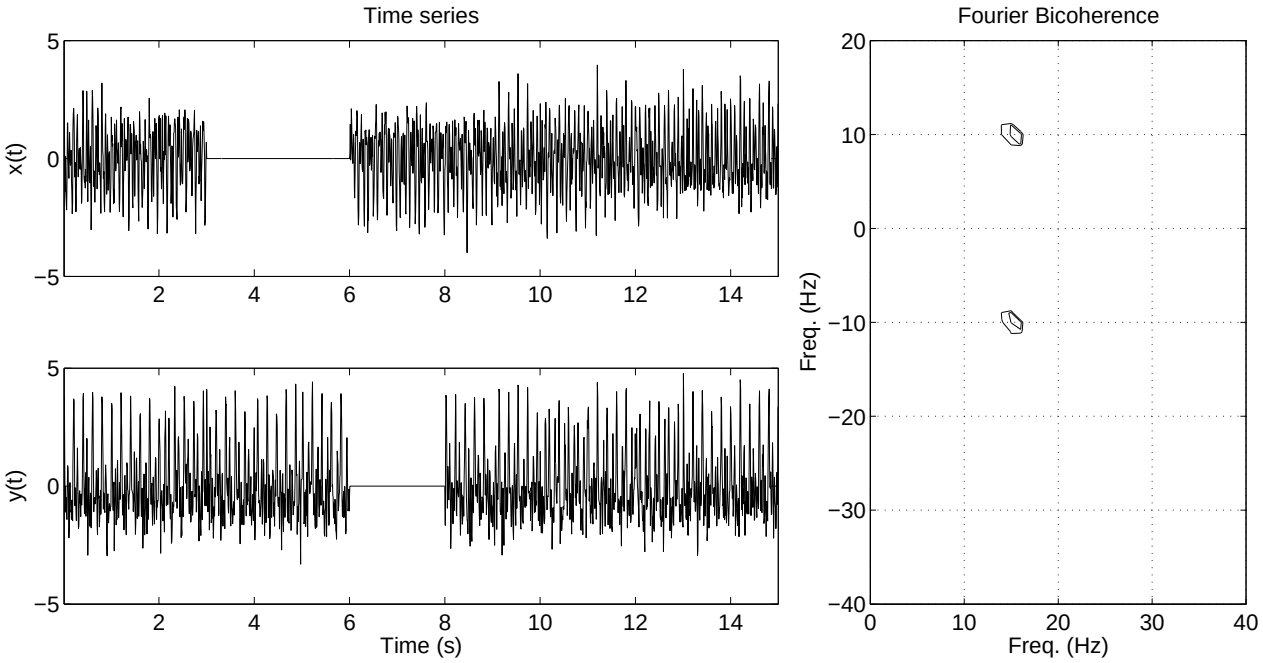

(a) (b)

Figure 2.18: Time series of an intermittently coupled system, input $x(t)$ top (a), and output $y(t)$ bottom (a), and Fourier-based cross-bicoherence (b)

The wavelet-based cross-bicoherence is used to identify intermittent coupling with the appropriate choice of the integration time. Three different integration times were chosen to demonstrate

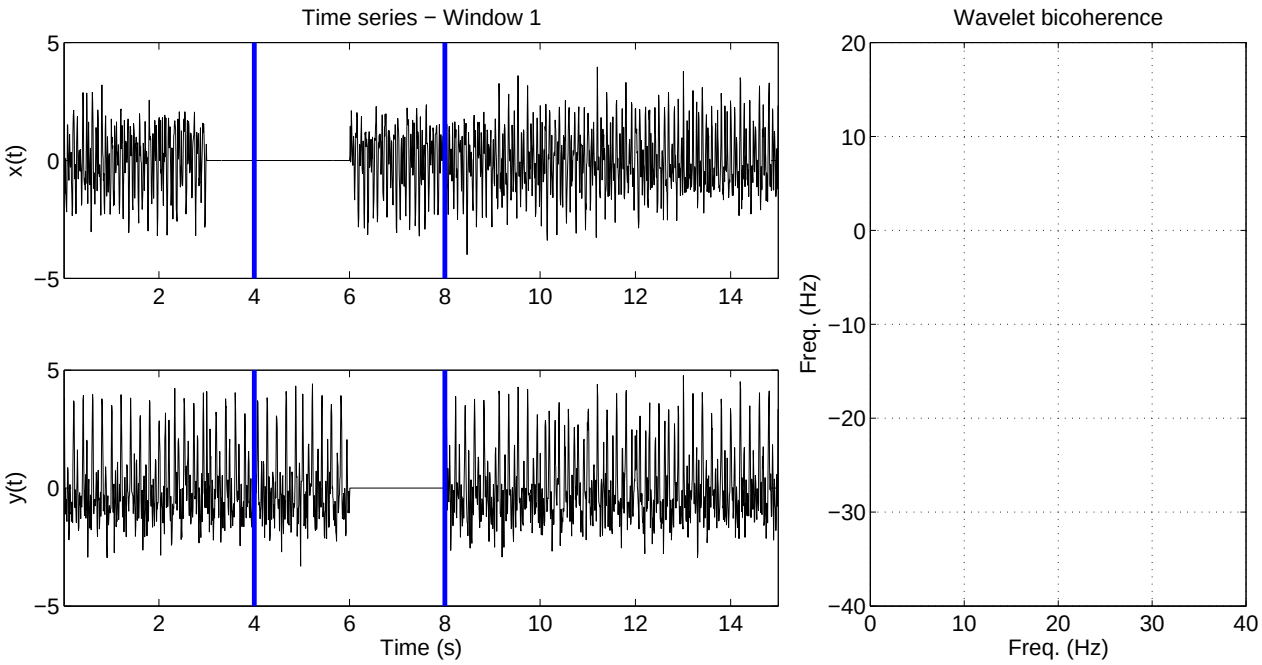

(a) (b)

Figure 2.19: Uncoupled interval; Integration window marked by blue lines (a), and resulting wavelet-based cross-bicoherence (b)

the intermittent coupling of this system. The first window spans $4s - 8s$ as shown in Figure 2.19a. During this interval, either $x(t)$ or $y(t)$ is always zero. The wavelet-based cross-bicoherence correctly identifies the uncoupled system by the absence of contours above 0.5 as shown Figure 2.19b. The next integration interval is chosen when the system is partially coupled, $7s - 10s$, as shown in Figure 2.20a. The wavelet-based cross-bicoherence of the system, shown with contour levels at $(0.5 : 0.1 : 0.9)$ in Figure 2.20b indicates partial coupling at $(15Hz, 10Hz, 25Hz)$ and $(15Hz, -10Hz, 5Hz)$. The final integration time is chosen when the system is fully coupled, $10s - 14s$, as shown with contour levels at $(0.5 : 0.1 : 0.9)$ in Figure 2.21a. The wavelet-based cross-bicoherence shows strong coupling at both $(15Hz, 10Hz, 25Hz)$ and $(15Hz, -10Hz, 5Hz)$.

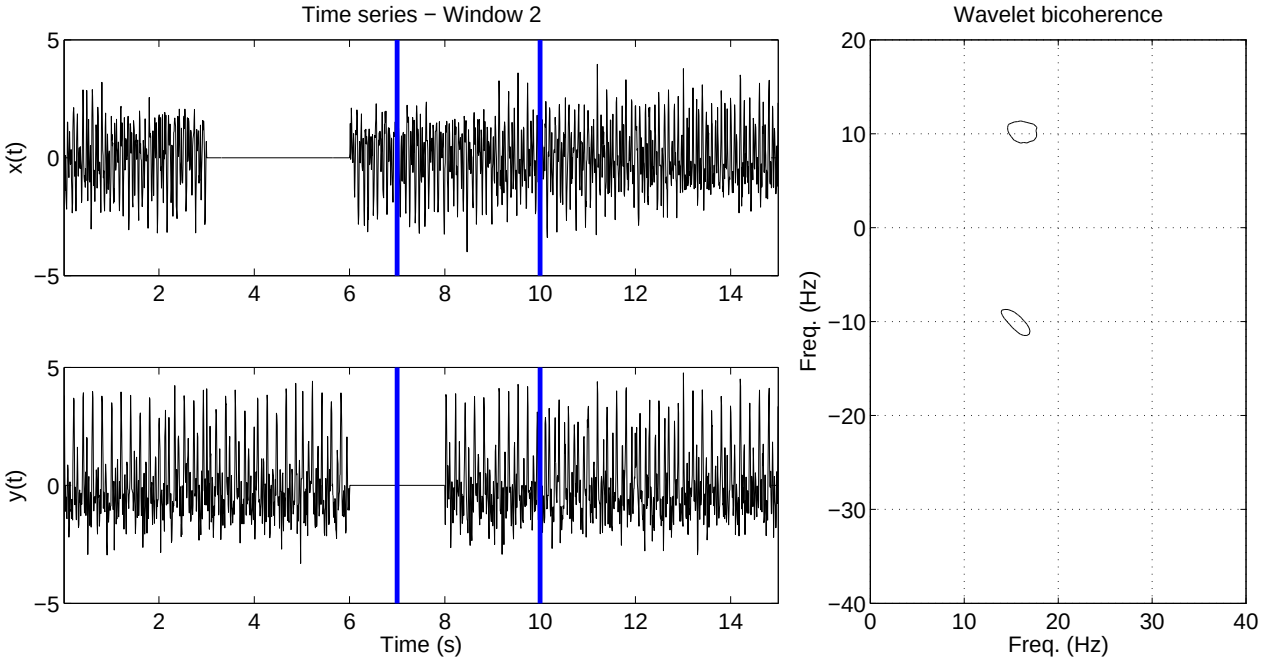

(a) (b)

Figure 2.20: Partially coupled interval; Integration window marked by blue lines (a), and resulting wavelet-based cross-bicoherence (b)

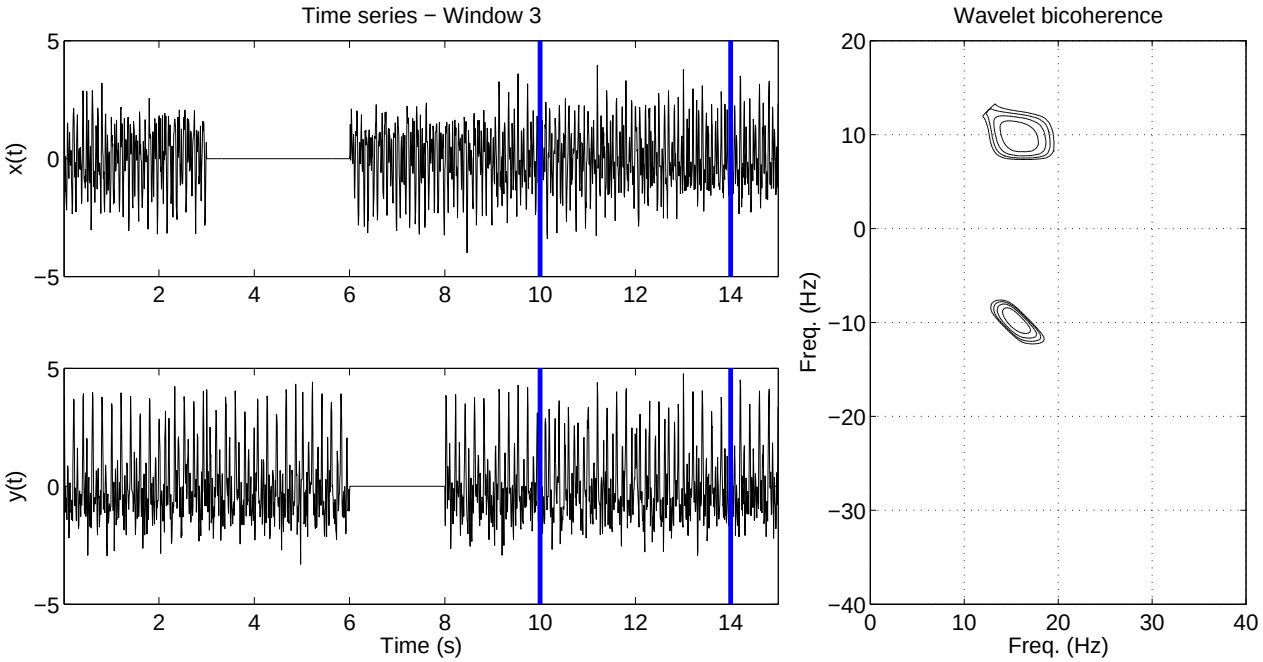

(a) (b)

Figure 2.21: Fully coupled interval; Integration window marked by blue lines (a), and resulting wavelet-based cross-bicoherence (b)